Using low-E resonators to reduce RF heating in biological samples for static solid-state NMR up to 900 MHz

Peter L. Gor'kov [a,*], Eduard Y. Chekmenev [a,c], Conggang Li [a,b], Myriam Cotten [d], Jarrod J. Buffy [e], Nathaniel J. Traaseth [f], Gianluigi Veglia [e,f], William W. Brey [a]

[a] *National High Magnetic Field Laboratory, Tallahassee, FL 32310, USA*
[b] *Department of Chemistry and Biochemistry, Florida State University, Tallahassee, FL 32306, USA*
[c] *Huntington Medical Research Institutes and California Institute of Technology, Pasadena, CA 91105, USA*
[d] *Department of Chemistry, Pacific Lutheran University, Tacoma, WA 98447, USA*
[e] *Department of Biochemistry, Molecular Biology and Biophysics, University of Minnesota, Minneapolis, MN 55455, USA*
[f] *Department of Chemistry, University of Minnesota, Minneapolis, MN 55455, USA*

Abstract

RF heating of solid-state biological samples is known to be a destabilizing factor in high-field NMR experiments that shortens the sample lifetime by continuous dehydration during the high-power cross-polarization and decoupling pulses. In this work, we describe specially designed, large volume, *low-E* ^{15}N–^{1}H solid-state NMR probes developed for 600 and 900 MHz PISEMA studies of dilute membrane proteins oriented in hydrated and dielectrically lossy lipid bilayers. The probes use an orthogonal coil design in which separate resonators pursue their own aims at the respective frequencies, resulting in a simplified and more efficient matching network. Sample heating at the ^{1}H frequency is minimized by a loop-gap resonator which produces a homogeneous magnetic field B_1 with low electric field E. Within the loop-gap resonator, a multi-turn solenoid closely matching the shape of the sample serves as an efficient observe coil. We compare power dissipation in a typical lossy bilayer sample in the new low-E probe and in a previously reported ^{15}N–^{1}H probe which uses a double-tuned 4-turn solenoid. RF loss in the sample is measured in each probe by observing changes in the ^{1}H 360° pulse lengths. For the same values of ^{1}H B_1 field, sample heating in the new probe was found to be smaller by an order of magnitude. Applications of the low-E design to the PISEMA study of membrane proteins in their native hydrated bilayer environment are demonstrated at 600 and 900 MHz.
© 2006 Elsevier Inc. All rights reserved.

Keywords: RF sample heating; Membrane protein; Dielectric loss; Loop-gap resonator; Flat-coil probe; Solid-state NMR probe; Lipid bilayers; Field in solenoid; Low-E; LGR

1. Introduction

Solid-state NMR experiments in conductive and dielectrically lossy protein samples are hindered by significant sample heating from high-frequency irradiation during cross-polarization (CP) and decoupling pulses [1–3]. Alternating electric currents induced in the conductive sample by the RF coil heat the sample internally during ^{1}H pulses [4–9]. This radio-frequency heating of biological macromolecules results in NMR lineshape distortions [10], a decrease in signal-to-noise (S/N) ratio [11], requires long recycle delays and can destroy the sample by dehydration.

Samples of mechanically aligned membrane proteins consist of hydrated lipid bilayers with varying buffer concentration and low protein-to-lipid ratios. To aid S/N for these dilute samples, larger sample volumes are preferred and rectangular ("flat") double or triple-tuned solenoids

---

* Corresponding author. Fax: +1 850 644 1366.
  E-mail address: pgorkov@magnet.fsu.edu (P.L. Gor'kov).

are frequently employed as transmit/receive coils to maximize filling factor and sensitivity given the rectangular nature of the sample preparation [12–16]. While solenoids are sensitive and efficient, at higher frequencies they also generate considerable conservative electric field. Dielectric losses associated with conservative electric field were shown to be responsible for nearly all of the internal RF heating in membrane protein preparations [3]. Loss of sample hydration during multi-millisecond ^{1}H pulses is often observed in the form of water droplets forming on the interior walls of the sample container. Dehydration of a sample may distort the bilayer and/or protein structure and introduce inhomogeneous broadening in the spectrum. It may also cause a probe to de-tune and slowly lose S/N throughout the duration of an experiment [13]. The RF energy which is lost to sample heating leads to degradation of ^{1}H decoupling and CP efficiency, with larger sample volumes only exacerbating this problem. A previously reported $8 \times 6 \times 12$ mm flat-coil solenoid [16] sees its ^{1}H RF field drop by a factor of 2 at 600 MHz with certain hydrated bilayer preparations (An example of decoupling heating inside a typical sample is given in Section 2.3 below). Variations in bilayer hydration and salinity are therefore highly inconvenient because each sample change requires a significant amount of spectrometer time for restoration of optimal CP conditions. In addition, the RF circuit may be unable to accommodate large tuning shifts and changes in Q upon loading different samples. This may limit the range of sample preparation techniques or require frequent circuit modification.

Various approaches to minimize sample RF heating have been described in the literature. Invasive techniques from solution NMR that minimize inductive resistance by sample concentrating [17,18] or using low-conductivity buffers [18] require serious sample modifications and are unsuitable for oriented lipid samples. When circumstances allow, freezing the sample can slow molecular motions responsible for the dielectric loss [19,1] and special hydration-controlled sample cells can be used to prevent lipids from dehydrating at lower frequencies [13]. Shielding conservative electric fields with Faraday shields is a common practice in probes for solution NMR and in coils for MRI [6,20]. However, when used within multi-turn solenoids in solid-state experiments, the reduction in self-resonant frequency brought by distributed capacitance between the windings and the Faraday shield limits both the ^{1}H frequency and the sample size. Alternatively, reducing the inductance of the coil can decrease the conservative electric field over the sample. The easiest way to lower inductance of a solenoid is to reduce the number of turns. An equivalent to the single turn solenoid, the loop-gap resonator [21–25] has been used in MRI and *in vivo* spectroscopy but has found limited use in solid-state NMR [26,27]. A scroll [28] is another example of a relatively low-inductance coil that shifts conservative electric fields to the outside of the sample area by the nature of its geometry [29,30]. Despite often

excellent performance at high frequency, the use of low-inductance coils in a multiply tuned coil network leads to inefficient performance at lower frequencies such as [15]N. Scrolls, in particular, are limited in sample volume because distributed capacitance between successive turns brings down their self-resonant frequency. Such side effects make low-inductance coils less desirable for sensitivity-limited experiments such as ^{15}N detection in dilute proteins, where larger sample volume and efficient low-frequency channels are often required.

It can be argued that some of these challenges arise from the practice of using the same coil for both high and low frequencies. A justification for using a single sample coil has been to produce equal spatial RF field profiles for both frequencies in CP experiments. However, Paulson and colleagues [31] have shown that significant CP field mismatch in a double-tuned solenoid coil occurs when its electrical length becomes comparable to 1/4 of the ^{1}H wavelength, making the above argument irrelevant for the combination of high-field strengths *and* large sample volumes described in this manuscript. A cross-coil probe design becomes more attractive at higher fields [9] and allows each coil to address its frequency-specific tasks, permitting substantial simplifications in the RF circuit. Commercially available cross-coil probes have been developed to reduce decoupler heating in high-field magic angle spinning applications and have recently been compared favorably to solenoids and scroll probes [9]. These probes are designed for smaller samples and use a different design for the resonators and matching network than described here.

We present here large volume flat-coil low-E probes developed for ^{15}N studies of dilute oriented membrane protein samples at fields up to 900 MHz. Instead of using a single double-tuned coil, these probes employ separate orthogonal resonators optimized to perform at their respective frequencies. A low-inductance loop-gap resonator reduces RF heating of biological samples and provides excellent B_1 homogeneity at the high ^{1}H frequency, while a multi-turn solenoid secures efficiency for the ^{15}N observe channel. We describe the design for an interchangeable [1]H–[15]N sample coil assembly and the rest of the probe circuitry. A hydrated, dielectrically lossy bilayer sample is used to quantitatively compare internal sample heating at 600 MHz in the new low-E probe and in a previously reported comparable probe with a single sample solenoid [16]. Functionality of the new probes is demonstrated by two-dimensional [15]N–[1]H PISEMA spectroscopy performed at 600 and 900 MHz. Three significant membrane protein systems are used here to demonstrate the capabilities of the probe design. The first two are sarcolipin (SLN) and phospholamban (PLN), 31 and 52 amino acid residue integral membrane proteins, respectively, expressed in cardiac muscle and involved in the regulation of calcium trafficking through direct inhibition of Ca^{2+}ATPase [32,33]. The third system is piscidin-3 (P_3-NH_2), a 22 amino acid long antimicrobial peptide found in mast cells from fish [34–37]. Low-E probes have made it possible to repeatedly

study without damage these and other samples of aligned membrane proteins at 900 MHz.

2. Methods

2.1. Sample cell

The preparation of mechanically oriented membrane samples is described in detail in our previous article [16]. The new probes described in this manuscript are designed for the same sample preparation with one exception. The original rectangular sample container was made in-house and had outer dimensions of 8×6 mm and a wall thickness of 1 mm. New Era Enterprises has since developed a thin-wall Pyrex sample cell that accommodates the same glass slides. The New Era cell walls are 0.5 mm thick, which reduces the outer dimensions to 7.5×5.5 mm for better filling factor. The sample volume inside expanded a little, making room for $\sim 10\%$ more slides than before. Sample clearance in the new probes has been reduced accordingly, resulting in 25% overall improvement in filling factor for the observe channel. The sample cells are factory-sealed at one end while the other end is sealed with beeswax. These sample cells are available from New Era Enterprises, Vineland, NJ, p/n SK-190505-1.

2.2. Measuring RF losses due to internal sample heating

A convenient way to quantify the extent of RF sample heating in a given probe is to compare the values of RF input power required to produce identical 90° pulse lengths in a lossy biological sample (P_{bio}) and in a non-lossy reference (P_{nl}). The power P_{nl} delivered to the probe with a non-lossy sample is dissipated in the coil inductor and other circuit components such as isolation traps, capacitors, and connecting leads. RF loss in each component is proportional to the square of voltage across it, which means it follows the square of the B_1 field produced in the sample coil. The biological sample adds dielectric (P_e) and conductive (P_m) losses induced by the conservative and non-conservative electric field components, respectively [5,6]. Assuming for the moment that, for the same B_1, loss in the probe circuit itself is the same for the two samples, the difference in input power $P_{heat} = P_{bio} - P_{nl} = P_e + P_m$ must then end up heating the biological sample. The same measurement can be done more precisely by comparing 90° pulse lengths (or RF fields $f_1 = \omega_1/2\pi$) measured with a lossy sample (τ_{90bio}) and with a non-lossy reference (τ_{90nl}) at the same power level P_{in}. Holding P_{in} constant eliminates the effect of errors that often accompany measurements of pulsed RF power. In the latter case, the fraction of RF input power diverted to sample heating can be expressed as:

$$\alpha_{heat} = \frac{P_e + P_m}{P_{bio}} = 1 - \frac{\tau_{90nl}^2}{\tau_{90bio}^2} = 1 - \frac{f_{1bio}^2}{f_{1nl}^2}. \qquad (1)$$

The loss factor α_{heat} alone should not be used to compare sample heating in different probes with different coils, or at different frequencies. A less efficient probe circuit with the same loss factor will deposit more power into the sample while achieving the same RF field f_1. For a heat sensitive sample, a spectroscopist should choose a probe with minimal heat deposition $q_{heat} = P_{heat}/f_{1bio}^2$, which is the cost of producing the required RF field f_1 in terms of power P_{heat} deposited in the sample. The heat deposition coefficient q_{heat} combines sample loss factor α_{heat} with probe circuit power efficiency η in the absence of sample loss:

$$\eta = \frac{f_{1nl}^2}{P_{in}},$$

$$q_{heat} = \frac{\alpha_{heat} P_{in}}{f_{1bio}^2} = \frac{\alpha_{heat}}{1 - \alpha_{heat}} \frac{P_{in}}{f_{1nl}^2} = \frac{\alpha_{heat}}{(1 - \alpha_{heat})\eta}. \qquad (2)$$

Because heating losses in the sample are proportional to E^2, $\sqrt{q_{heat}}$ is proportional to E/B_1 (at constant irradiation frequency), a parameter conveniently derived from coil simulations that can be used to compare the suitability of different sample coils [9].

As noted above, the simple measurement of α_{heat} in Eq. (1) is correct only if the presence of a lossy sample does not redistribute losses between the probe's isolation traps and other components. This assumption is valid as long as v/f_1 (volts per kHz) across the lossy circuit components remains unchanged, which is true for probe circuits where one side of the coil is grounded. However, for a balanced or partially balanced solenoid with the zero voltage node set somewhere between its ends, the ratio of voltages at opposite ends of the coil determines the relative loss contributed by each side of the circuit. Sample-to-sample retuning of the probe may shift the voltage node along the coil and change the power dissipated in the various circuit components. As a rule, we balance the ^1H circuit before each τ_{90} measurement to maintain equal voltages at the ends of the coil [16].

We suspect that the RF loss mechanism in the mechanically aligned membrane sample might not be accurately modeled by a saline sample. The membrane sample, consisting of repeated layers of glass plates, lipid membranes, and buffer, may have an average dielectric constant considerably smaller than bulk water. Also, the membrane sample may be subject to RF losses caused by oscillating dipoles interacting with the ^1H electric field, in addition to the expected ion conductivity. The contribution to RF loss from oscillating dipoles has its maximum at the critical frequency $\omega_c = 1/\tau$, where τ is a dipole's correlation time. In bulk water ω_c is very high (~ 20 GHz) and such contribution is minimal. But correlation times of constrained water molecules in the interfacial region of the lipid bilayers are 10–100 times shorter [38–40], resulting in more efficient RF power absorption. For this reason, we use a typical bilayer sample preparation serving as a lossy biological reference in our measurements of α_{heat}.

To prepare the reference sample, 100 mg of lipids (DMPC:DMPG in 3:1 molar ratio) were dissolved in organic solvent and deposited onto $5.7 \times 12 \times 0.03$ mm glass slides. Once the solvent had evaporated, drops of phosphate buffer (100 mg total) at pH 6.0 were added to each slide, resulting in a ~50% hydration level and ~40 mM phosphate buffer concentration. The slides were then stacked and the stack was inserted into the sample cell. The resulting stack of sample slides occupied the maximum volume available in the sample cell container. Another rectangular cell containing $6 \times 4 \times 9$ mm of 100% neutral paraffinic oil served as a non-lossy reference sample. The difference in dielectric constant of the lossy and non-lossy samples may vary the electrical length n_λ of the loaded sample coil and the v/f_1 values at its ends. A significant difference in n_λ would therefore change the loss in the isolation traps and tuning components in spite of balancing. To verify the appropriateness of Eq. (1), the electrical length of the coil was measured with each reference sample. To determine n_λ of the loaded coil, its lowest self-resonance frequency f_{SR} was measured with both ends afloat. This frequency, obtained with a Vector Network Analyzer (VNA) and a pickup loop, corresponds to the $\lambda/2$ excitation mode which has a zero voltage node in the middle and zero current at the ends. The number of wavelengths n_λ in the loaded coil at operating frequency f is then $n_\lambda = f/2f_{SR}$. For the sample coils discussed and compared in this manuscript by means of Eqs. (1) and (2), the difference in the electrical length when loaded with above reference samples did not exceed 5% (see Section 3), a shift that should not have a significant effect on the loss in the probe circuit, and which we can safely neglect.

2.3. Extent of internal sample heating

To illustrate the extent of the heating problem where lipid bilayer samples are concerned, we refer to the previously reported 600 MHz ^{15}N–^{1}H solenoidal flat-coil probe [16], which is a balanced variation of the double-tuned Cross–Waugh design [41] using a 4-turn, $8 \times 6 \times 12$ mm rectangular solenoidal sample coil. Input power of 65 W was needed to obtain a ^{1}H f_1 value of 50 kHz in a paraffinic oil reference (note that in terms of size *and* frequency ($n_\lambda = 0.27$) this solenoid is larger than most flat coils used in other laboratories). In the same article, we reported a preparation of piscidin-1 peptide in oriented hydrated lipid bilayers (DMPC:DMPG, 3:1 molar ratio, 20:1 lipid:peptide ratio, hydration level ~50%, total sample weight ~200 mg deposited on 55 $5.7 \times 12 \times 0.03$ mm glass slides at pH 6.0 in phosphate buffer). When loaded into the coil, this sample reduced the ^{1}H channel efficiency by a factor of 2. Obtaining the same level of ^{1}H decoupling field for this lossy sample required ~260 W of input power, meaning that 195 W or 75% of the input ^{1}H power heats the biological system. Assuming a sample heat capacity of 3.5 J/g °C [3], and considering that ^{1}H decoupling pulses are too short for any substantial heat transport to take place, the increase in

sample temperature during a single 10 ms, 50 kHz decoupling pulse can be estimated as $\Delta T = 195 \times 0.01/(3.5 \times 0.2) = 2.8$ °C. In our experience with this probe and sample, long recycle delay times and ample cooling air were required to avoid damage to the bilayers. Still, these measures did not guarantee that the set temperature was in fact the sample temperature and that there were no temperature gradients across the sample. To carry out repeatable and non-destructive experiments over a wide range of sample hydration and salinity with this and with more lossy samples, one must attempt to reduce the magnitude of the high-frequency electric field interacting with the sample inside the RF coil.

2.4. Electric field in the solenoid

It has been demonstrated recently [3] that the conservative part of the electric field ($\nabla \times \vec{E}_c = 0$) is responsible for nearly all of the RF heating experienced by sample cells of aligned membrane proteins. If we could reduce the conservative electric field E_c without affecting the desired magnetic field B_1, problems of sample heating would be alleviated. Reducing the number of turns is a straightforward route to minimizing the conservative electric field in a sample solenoid. In an elongated solenoid where length is larger than diameter, the conservative electric field is approximately just the driving voltage applied to the terminals of the solenoid divided by its length. For a solenoid of length l and inductance L operating at Larmor frequency ω, with driving voltage $\omega L I$,

$$E_c = \frac{\omega L I}{l}. \tag{3}$$

For a finite single-layer solenoid wound on a former of any cross-section, the axial component of magnetic field generated by current I at point $\vec{r}$ (see Appendix A) is given by

$$B_x(\vec{r}) = \mu_0 i \frac{\Omega}{4\pi}, \tag{4}$$

where $i = NI/l$ is the linear current density, N is number of turns in the coil, and Ω is the solid angle subtended by the coil winding at observation point $\vec{r}$. Neglecting wavelength effects at the Larmor frequency ω, the current amplitude required to generate a target RF field $f_1 = \omega_1/2\pi$ (in Hz units) is given by

$$I = \frac{8\pi f_1 l}{\gamma \mu_0 N \Omega}, \tag{5}$$

where γ is the gyromagnetic ratio of the nucleus. Combining Eqs. (3) and (5) gives us an expression for the suitability of the RF coil: the ratio of conservative electric field to magnetic field:

$$\frac{E_c}{f_1} = \frac{8\pi L B_0}{\mu_0 N \Omega}. \tag{6}$$

If we make the approximation that $L \sim N^2$, the expression becomes

$$\frac{E_c}{f_1} \propto \frac{NB_0}{\Omega}, \tag{7}$$

and so it is clear that reducing the number of turns reduces sample heating for a given B_1 field.

The expression $\omega L I$ for voltage in the above equations neglects wavelength effects and so applies to coils operating significantly below self-resonance. As the solenoid electrical length increases and its self-resonance frequency approaches the Larmor frequency, coil impedance will increase as well, adding further to the electric field. This is yet another reason to minimize the number of turns. A single-turn solenoid made from a wide conductive strip, also known as a loop-gap resonator (LGR), will reduce RF losses considerably and is known to provide excellent B_1 homogeneity [26,27]. Use of a coil with such low-inductance in a multi-tuned circuit, however, will lead to excessive power dissipation in stray leads and trap inductors, and may result in diminished efficiency, especially in the low-frequency channel. Since sample dielectric loss depends strongly on frequency [6,8,29,9], the vast majority of sample heating occurs from RF irradiation at the ^{1}H frequency. It makes sense therefore to implement this low-E coil for the ^{1}H decoupling channel and retain a multiple turn solenoid as an efficient observe coil for lower frequencies where sample heating is of minimal concern.

2.5. Details of the sample coil assembly

The ^{15}N–^{1}H flat-coil probes presented here utilize separate orthogonal RF coils, each optimized to perform at its respective frequency and driven by a balanced single-reso-nance circuit. The outer low-E ^{1}H coil is a rectangular loop-gap resonator (Fig. 1A) that produces a magnetic field along the y-axis. It is made from 0.35 mm thick, 14.2 mm wide copper strip formed around a 15×9 mm rectangular block. The ends of the strip are terminated by non-magnetic chip capacitors (100B series, American Technical Ceramics) completing the LGR. Low-inductance leads soldered at both sides of the gap provide both electrical connections and mechanical supports for the free-standing resonator, which is connected to the ^{1}H matching network below by means of two non-magnetic brass screws (Fig. 3A). The inner, ^{15}N observe coil is a 5-turn $7.7 \times 5.7 \times 11$ mm ID rectangular solenoid, which is placed next to the sample in order to maximize sensitivity. The solenoid is made by forming round copper wire of 0.8 mm diameter (American Wire Gauge 20) into grooves in a collapsible rectangular 7.6×5.6 mm block. The block is then removed, leaving a rectangular coil that closely matches the size of the sample cell for best filling factor. The resulting air gap between the wires in the solenoid is 1.2–1.3 mm. Thin 0.8 mm slides made from low-loss dielectric (Rexolite™, Boedeker Plastics, Inc., Shiner, TX) are affixed to the top and bottom of the inner observe solenoid by drops of epoxy (H54 epoxy, Epotek, Inc., Billerica, MA). The Rexolite plates hold the solenoid in the correct position and reduce the chance of arcing to the LGR. During final assembly, the solenoid is slid into the outer ^{1}H resonator so that the leads come out on the same side in the horizontal (x–y) plane as depicted in Fig. 1A. There they are terminated by flat washers that are screwed to elevated terminal posts that connect to the ^{15}N circuit below the Teflon variable temperature chamber (Figs. 3A, 6). The
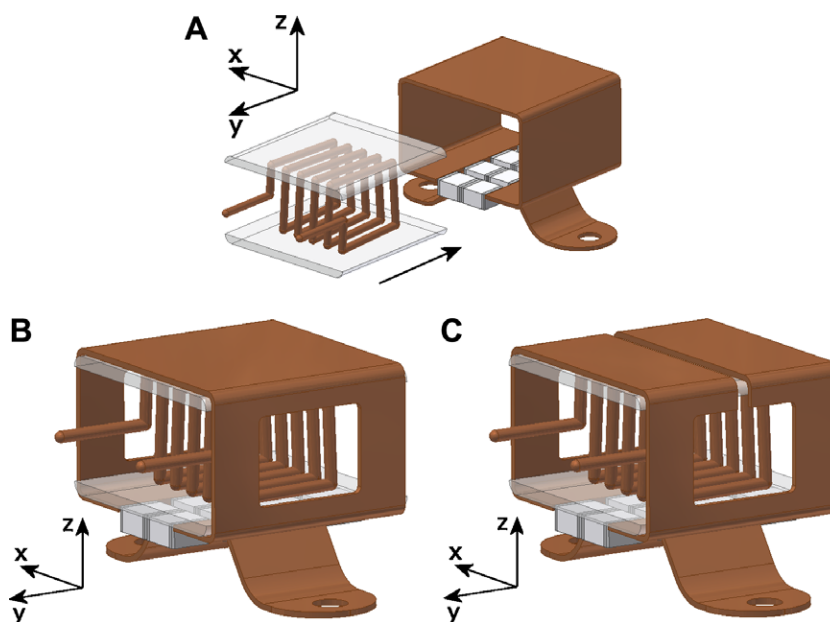

Fig. 1. Mechanical design of the ^{1}H–^{15}N low-E flat-coil assembly: (A) ^{15}N observe solenoid is inserted orthogonally inside the ^{1}H loop-gap resonator; (B) side windows are cut in the loop-gap resonator for sample insertion along x-axis; (C) a slot is cut on top of the ^{1}H loop-gap resonator to reduce ^{15}N eddy currents.
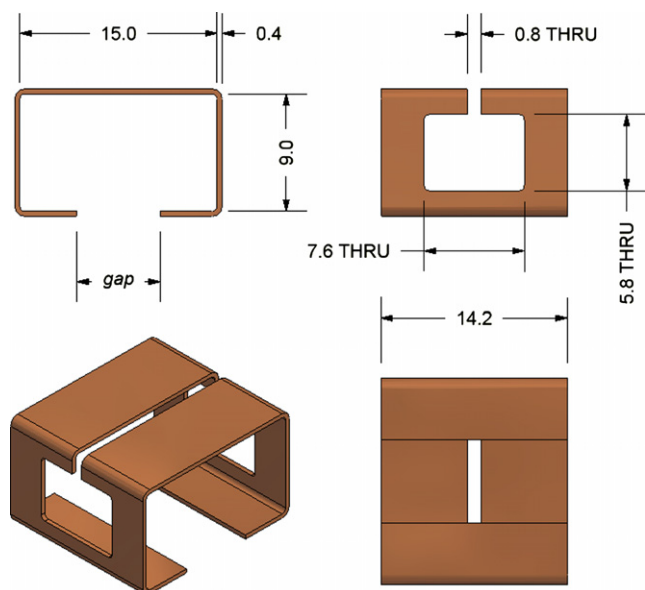
Fig. 2. Dimensions for the ^{1}H loop-gap resonator. Parameter *gap* depends on the number and size of chip capacitors employed in the resonator.

inner, 125 nH solenoid produces its magnetic field in the x-direction, orthogonal to the y-axis field of the LGR.

The ^{1}H resonator used in this cross-coil assembly is essentially a 1-turn rectangular solenoid wound orthogonally around the ^{15}N solenoid. The obvious dilemma posed by such an arrangement (Fig. 1A) is how to place samples inside if both ends of the ^{15}N coil are blocked by LGR. To address this issue, two rectangular windows (7.6 × 5.7 mm) were cut in the opposite sides of the ^{1}H resonator to allow unobstructed sample insertion along the x-axis (Fig. 1B). In addition, a 0.8 mm slot in the top of the ^{1}H resonator (Fig. 1C) was added to reduce eddy currents induced by the observe solenoid, as further explained in the next section. Fig. 2 shows the exact physical dimensions of the ^{1}H coil form. The parameter *gap* depends on the arrangement of fixed capacitance and is discussed further in Section 2.7. The resulting ^{1}H coils have an inductance of about 10 nH. It is worth noting that while we derived

the shape of our loop-gap resonator from a wide single-turn solenoid, one can arrive at a similar geometry by starting with the Alderman–Grant coil [20] and modifying it as was done in an application to ESR force microscopy [42].

Note that the use of solderless terminal connections allows for fast switching between coil assemblies of various sizes and geometry. A flat-coil assembly with the sample opening rotated by 90° (Fig. 3B) allows information about other components of the chemical shift tensor to be obtained, while a scaled-down assembly using a 6-turn 7 × 3 × 9 mm inner solenoid may be useful for preparations where sample quantities are limited (Fig. 3C).

2.6. Reducing ^{15}N eddy currents in low-E resonator

Alternating flux from the ends of the ^{15}N solenoid shown in Fig. 1B will induce eddy currents as it passes through the sample access windows of the ^{1}H resonator. Eddy currents will tend to flow around the rectangular windows on the inside and outside of the resonator, counteracting the RF field produced by the ^{15}N solenoid and thereby reducing the ^{15}N B_1 over the sample. Consider, for example, contour A_W that traces the edges of the window in plane $x = x_0$ and is collinear with the x-axis as shown in Fig. 4A. Let $\Phi_W(x_0)$ be the flux through that window. The electromotive force (emf) induced around A_W on either side of the window by an alternating ^{15}N field B_1 is given by

$$\text{emf}(x_0) = -\frac{\partial \Phi_W(x_0)}{\partial t} = -\frac{\partial}{\partial t} \int \int_{A_W} \vec{B}_1(x_0, y, z) \cdot \hat{n}(x_0) \, dz \, dy$$

$$= \omega_{15N} \Phi_W(x_0).$$

Together with the opposing window at $x = -x_0$, these co-rotating eddy currents form a "Helmholtz" pair along the x-axis.

To interrupt the path for eddy currents, a narrow slot was placed along the top of the ^{1}H resonator, merging two windows into a single opening as shown in Figs.
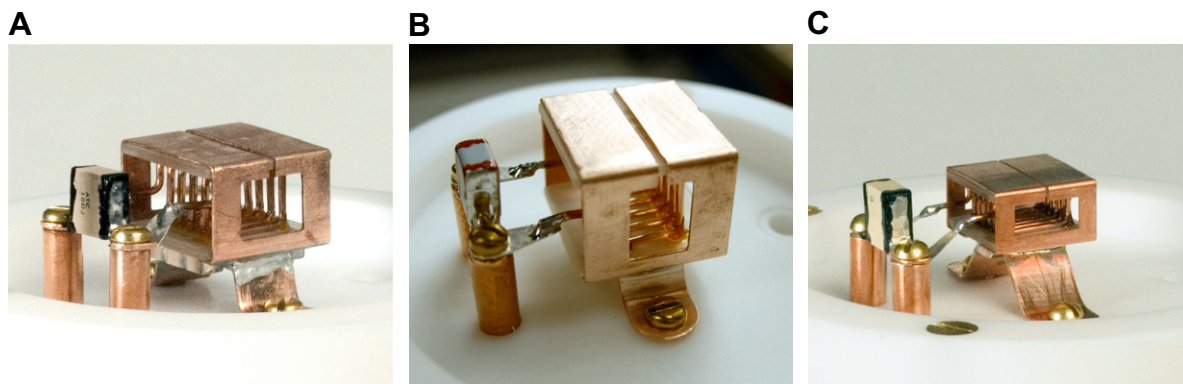

Fig. 3. Photographs of different low-E cross-coil assemblies: (A) horizontal flat-coil structure with 7.5 × 5.5 × 11 mm sample aperture; (B) vertical flat coil—with the sample opening rotated by 90°; (C) small flat coil for sample-limited preparations with 7 × 3 × 9 mm sample aperture. Coil assemblies are interchangeable by means of four non-magnetic brass screws.
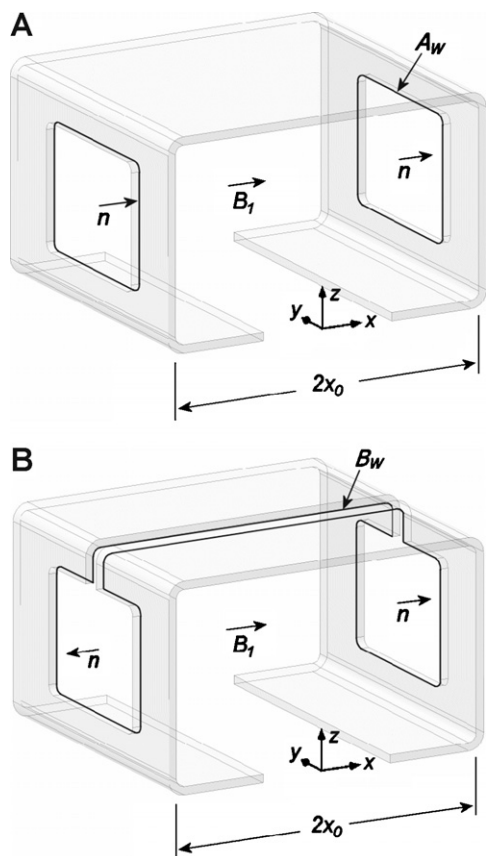
Fig. 4. Illustration for discussion of ^{15}N eddy current reduction in ^{1}H resonator. ^{15}N observe solenoid is not shown for clarity—its B_1 field direction along the x-axis is highlighted.

1C, 2, and 4B. The emf around the merged contour B_W consisting of both windows and a slot (Fig. 4B) is the sum of emf around individual windows. The normals to the opposite windows in contour B_W are of different signs $\hat{n}(-x_0) = -\hat{n}(x_0)$, resulting in $\Phi_W(-x_0) = -\Phi_W(x_0)$ and

$$\text{emf} = \omega_{15N}\Phi_W(-x_0) + \omega_{15N}\Phi_W(x_0) = 0.$$

Since the net emf around B_W vanishes, we can conclude that slotting the ^{1}H resonator prevents ^{15}N eddy currents from forming around the sample windows. This cancels current induced in the outer surface of the resonator and reduces eddy currents that form inside. Residual eddy currents are still expected to form on the inside

Table 1
Reducing ^{15}N eddy current loss in the ^{1}H coil

^{1}H coil	^{15}N τ_{90} (μs)	Power lost to eddy currents	Extra power to compensate loss
None	5.3	—	—
Fig. 1B	7.3	47%	+90%
Fig. 1C	6.0	22%	+28%

^{15}N 90° pulse lengths were measured using ^{15}N-labeled glycine at 240 W of input power.

of the wide window frames at $x = \pm x_0$ and within the top resonator strips that are in close proximity to the solenoid wire. NMR measurements were conducted to determine the loss in ^{15}N B_1 due to the proximity of the LGR. The results are summarized in Table 1. Introducing the outer ^{1}H resonator with two separate sample windows (Fig. 1B) caused a 27% drop in ^{15}N B_1 at 60.8 MHz and required almost doubling the RF power to match the B_1 field of the ^{15}N solenoid alone. Merging the sample windows with a slot along the top of the ^{1}H resonator (Fig. 1C) reduced the induced eddy currents enough to recover more than half of the ^{15}N power efficiency (kHz^2/W) that was lost to the ^{1}H resonator. We conclude that while slotting the LGR does not completely eliminate ^{15}N loss associated with coupling to the observe solenoid, it does reduce such loss to an acceptable level.

2.7. RF circuit for 600 MHz low-E probe

The intrinsic isolation between channels provided by orthogonal resonators greatly reduces the need for isolation traps and the loss associated with these traps, often the dominant source of RF loss in a single coil probe. Instead, each coil can be driven by an optimized single-resonance circuit. The RF circuitry employed in the 600 MHz low-E probe is illustrated in Fig. 5. The thick outline represents a rectangular single-turn ^{1}H coil L_0 that surrounds the observe solenoid L_1. Tuning and matching of the ^{1}H channel is accomplished by adjusting variable capacitors C_3 and C_1, respectively. Another variable capacitor C_2 is a symmetry load responsible for balancing the low-E resonator. Although the resonator loop is too short for ^{1}H wavelength effects to be of significance, balancing equalizes the voltage at the ends of the ^{1}H coil L_0 and so reduces the probability of arcing [43,31,16]. Symmetry capacitor C_2 is adjusted to center the virtual ground in the middle of the
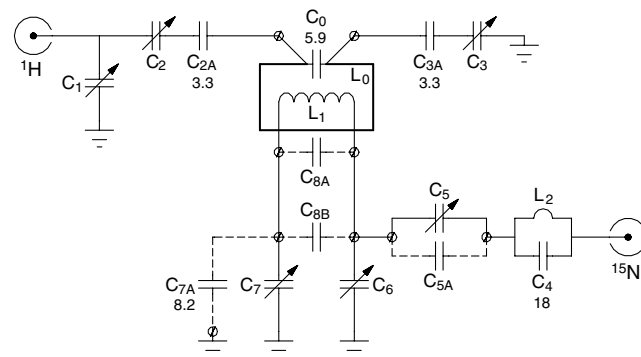

Fig. 5. RF circuit of the 600 MHz low-E ^{15}N–^{1}H flat-coil probe. The low-E coil assembly consists of a 5-turn rectangular ^{15}N observe solenoid L_1 inside a low-inductance ^{1}H loop-gap resonator $L_0 - C_0$ (thick outline). Coil inductance values are $L_0 \approx 10$ nH, $L_1 \approx 125$ nH. Dashed lines represent detachable capacitors that allow retuning to other observe nuclei. The sum of values of chip capacitors ($C_{8A} + C_{8B}$) is about 45 pF for the ^{15}N circuit.

[1]H coil inductor, as described previously [16]. Probing the virtual ground is done through the exhaust hole on top of the VT sample chamber, with the RF shield cover closed. A pair of 0.3–3 pF variable capacitors are used for C_2 and C_3 (RP-VC3-6, Polyflon Co., Norwalk, CT), while a 1–25 pF variable capacitor is used for C_1 (NMAT25HV, Voltronics Corp., Denville, NJ).

Although a single-turn solenoid L_0 may reduce sample heating, it will only be efficient if the main ^{1}H tuning capacitance C_0 is mounted directly across it and the resonant frequency of the resulting loop-gap resonator is brought very close to the ^{1}H frequency. Otherwise, RF losses in coil leads, terminal posts and other stray conductors including screws inside variable capacitors will greatly diminish ^{1}H channel efficiency. Power loss in these elements is proportional to I_S^2, where I_S is the stray current flowing through C_1, C_2, and C_3, outside of the loop $L_0 - C_0$ that contains the sample. The ratio of stray current to current I_0 in inductor L_0 that generates the [1]H B_1 field in the sample is given by

$$\frac{I_S}{I_0} = 1 + j\omega C_0 (R_0 + j\omega L_0) = 1 - \frac{\omega^2}{\omega_0^2} + j\omega C_0 R_0$$

$$= 1 - \frac{\omega^2}{\omega_0^2} + j\frac{\omega}{\omega_0} Q_0^{-1}, \tag{8}$$

where ω is the [1]H Larmor frequency, ω_0 is the resonance frequency of the $L_0 - C_0$ loop, and R_0 is the resistance associated with it. R_0 includes resistive loss in sample inductor L_0, loss in the capacitor C_0, radiation loss, and can be estimated from measuring the Q of the resonator at frequency ω_0. From Eq. (8), stray losses are minimized when the resonance frequency ω_0 of loop $L_0 - C_0$ is brought as close to ω as feasible. The resonant frequency ω_0 was measured on the bench using a probing loop and a VNA. The values of the chips forming capacitance C_0 were adjusted until ($\omega_0/2\pi$) fell in a 10 MHz range (628 ± 5 MHz) slightly above the ^{1}H frequency. Essentially, the chips are used to pre-tune the coil while the rest of the matching circuit is used for fine tuning of the ^{1}H channel. By introducing C_0, the ratio of stray current to current in the coil is reduced to

$$\frac{I_S}{I_0} \approx 2\frac{\omega_0 - \omega}{\omega_0} + jQ_0^{-1} \approx 2 \times 28/628 \approx 0.09. \tag{9}$$

Current in the ^{1}H circuit is therefore highly localized to the $L_0 - C_0$ loop, drastically reducing the power loss in the outside matching network. The second term jQ_0^{-1} in Eq. (9) is much smaller than the first term within the above ω_0 range, indicating that loop $L_0 - C_0$ is not in fact self-resonant. The lower limit for ω_0 is set by the values and ranges of variable capacitors C_1, C_2, and C_3, and by the desire to provide a sufficient tuning range for the ^{1}H channel ($\sim$15 MHz). Because this probe is designed for interchangeable RF coils, the tuning range of its ^{1}H circuit must accommodate all reso-

nators whose $f_0 = \omega_0/2\pi$ falls in the specified 10 MHz range and allow for sample-dependent tuning shifts at the same time. A 15 MHz tuning range in a 600 MHz probe may be considered small under other circumstances, since a good ^{1}H tuning range is often required to counter shifts in probe resonance with different samples. Such shifts, however, are primarily the result of sample interaction with the ^{1}H electric field, which is substantially reduced in this coil. The ^{1}H resonance shifts observed in the 600 MHz low-E resonator are on average 5 times smaller than in a comparable flat-coil probe [16] that uses a double-tuned solenoid (see $\Delta f/f$ in Table 2).

When arranging for the C_0 capacitance, it is important to realize that because inductor L_0 has only one turn, C_0 will be subject to very high current. Since $\omega_0 \approx \omega$, the current experienced by C_0 inside the low-E resonator is $\approx I_0$ and can be easily estimated from Eq. (5). The total solid angle Ω subtended by the loop-gap resonator is about 3π (see Appendix A). Therefore, a ^{1}H RF field of 100 kHz, for example, requires a current I_0 of about 70 A. We arranged a number of chip capacitors in parallel across the gap in inductor L_0 in order to carry this relatively large current. The fixed non-magnetic chip capacitors we used in the early stages of development (25 and 11 series from Voltronics Corp., Denville, NJ) tended to fail after few hours of experiment, with the 25 series chips cracking apparently from internal heat build-up despite ample ventilation. In tests with a soldering iron, we observed that the chips from Voltronics required longer to cool than the otherwise similar non-magnetic chips (ATC 100C and 100B series) from American Technical Ceramics, Huntington Station, NY. Subsequently, we have used Voltronics chips only where current is limited. And although more prone to voltage breakdown than the physically larger 100C series, 100B chips actually have a smaller effective series resistance (ESR) that allows them to withstand higher currents and longer pulses. Their smaller case allows for grouping more chips in parallel which further decreases the ESR of the entire assembly. We used two variations of ^{1}H coil with gaps of 6.4 and 9.9 mm, each accommodating 4 parallel bridges of series-connected chip capacitors. The smaller gap accommodates capacitor bridges made of two series-connected chips while the larger gap is wide enough to fit three chips in series. The ^{1}H resonator with wider gap will therefore withstand more voltage and reach higher B_1 fields, albeit at the expense of somewhat lower efficiency. In this text we will refer to the 6.4 and 9.9 mm gap resonators as coils I and II, respectively. An additional coil III with smaller dimensions for use with sample-limited preparations (Fig. 3C) has only two chips arranged in parallel within its 3.0 mm gap. The chip capacitors employed in each resonator were screened for signs of residual magnetism occasionally found in the non-magnetic series made by ATC.

The ^{15}N observe circuit employs a 5-turn rectangular sample solenoid L_1 (125 nH) which provides better efficien-

Table 2
Sample heating comparison between the ^{1}H–^{15}N probes with low-E resonator and double-tuned 4-turn solenoid

Field f/MHz	Probe	^{1}H								^{15}N	
		τ_{90nl} μs 65 W	τ_{90bio} μs 65 W	α_{heat}	η kHz^2/W	q_{heat} mW/kHz^2	$\Delta f/f \times 10^{-3}$	f_1 limit kHz	$\frac{A_{810°}}{A_{90°}}$	f_1 kHz 700 W	$\frac{A_{810°}}{A_{90°}}$
400	4't solenoid	4.75	7.10	55%	42.6	**28.7**	−4.2	103[a]	76%	58	80%
600	4't solenoid	5.05	9.55	72%	37.7	**68.2**	−8.3	100[a]	71%	54	76%
600	Low-E coil I	5.10	5.48	13%	37.0	**4.0**	−1.5	76	93%	71	74%
600	Low-E coil II	5.75	6.23	15%	29.1	**6.1**	−1.5	100	95%	71	74%
900	Low-E coil II	6.88	8.45	34%	20.3	**25.4**	−3.6	60	80%	70	71%

α_{heat} is a fraction of ^{1}H input power lost to heating in the bilayer sample, η is probe power efficiency, and q_{heat} correlates loss in the sample with RF field magnitude (see Section 2.2). $\Delta f/f$ is ^{1}H resonance shift for bilayer reference. $\frac{A_{810°}}{A_{90°}}$ is B_1 homogeneity over $6 \times 4 \times 9$ mm volume. ^{15}N B_1 fields were measured with ^{15}N-labeled glycine.

[a] Sustainable in non-lossy sample only.

cy at its low 60.8 MHz operating frequency than an LGR. The solenoid is driven by a separate single-resonance balanced circuit that, as in the ^{1}H circuit, reduces by half the voltage at its ends and allows the coil to generate twice the RF field for a given voltage rating of its tuning capacitors. This makes it possible to use relatively smaller trimmer capacitors for C_5, C_6, and C_7 (NMNT10-6, 1–10 pF, Voltronics Corp., Denville, NJ). The observe nucleus can be easily changed by replacing one or more of the chip capacitors C_{8A}, C_{8B}, C_7, and C_{5A}, that are screwed to copper terminals located throughout the circuit (Fig. 6). Capacitors C_{8A} and C_{8B} are responsible for coarse tuning of the observe channel. These two 100C series chips localize low-frequency current to a short loop between the ends of the observe coil and minimize current flowing into the larger variable capacitors C_6 and C_7, which are used for finer tuning. Matching the observe circuit to 50 Ω is done with variable capacitor C_5. Additional capacitance C_{5A}, if needed for even lower observe frequency, may be screwed to the terminals in parallel with C_5. Tuning capacitors C_6 and C_7 have their extended shafts connected by a 3-gear mechanism to a single tuning rod that changes positions of both pistons at the same rate, expanding the range over which the observe channel can be tuned without re-adjusting circuit balancing and matching. For each observe nucleus range set by C_8, balancing of the solenoid is
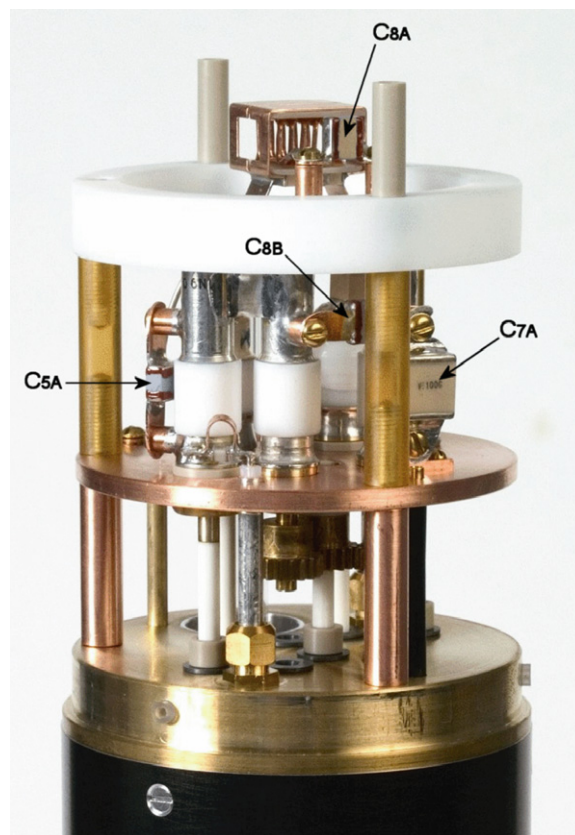

Fig. 6. Photograph of the 600 MHz low-E ^{15}N–^{1}H flat-coil probe (sample VT chamber removed for clarity). Arrows indicate locations of the screw-on capacitors in the low-frequency observe channel (see Fig. 5).

accomplished by affixing the proper chip capacitor C_{7A} in parallel with the variable trimmer C_7. To verify the alignment of lipid bilayers via ^{31}P detection, the low-frequency channel may be retuned to 242 MHz by removing all chip capacitors and by placing a matching inductor in parallel with C_5.

Fixed tuning capacitors C_{8A} and C_{8B} are subject to the highest current and voltage amplitudes in the ^{15}N circuit. The achievable RF field f_1 in the ^{15}N channel is therefore limited by their ability to withstand these adverse conditions during milliseconds-long pulses. Using Eq. (5) and the formula for solid angle from Appendix A, the peak current amplitude I required to generate an f_1 of just 50 kHz in the ^{15}N solenoid ($\Omega \approx 3.3\pi$) is approximately 48 A. To split the current and to reduce the possibility of heat build-up in capacitors C_8 when operating at high f_1 fields, it is prudent to select chips C_{8A} and C_{8B} with similar values. Using two chips of smaller value in parallel reduces the total ESR and results in less internal heating. At $f_1 = 50$ kHz, the voltage amplitude across the capacitance C_8 is $\omega L_1 I = 2\pi \times 61 \cdot 10^6 \times 125 \cdot 10^{-9} \times 48 \approx 2.3$ kV, close to the 2.5 kV declared voltage rating of the 100C series ATC chip. During initial tests, a corona formed at the termination plates of capacitors C_8 shortly before the ^{15}N RF field reached 50 kHz in 2 ms long pulses. Fortunately, the arcing discharge chose a path through the air which is less destructive to the chip than a path through the dielectric. Attempts to use a larger 100E series chip rated to withstand more voltage (3.6 kV) yielded no improvement in achievable RF field, suggesting that voltage gradients formed around these chips that exceeded the relatively poor dielectric strength of the room air. On close inspection, one can note the presence of conductive bands around the capacitor termination plates that extend toward the center of the capacitor by ≈ 1 mm (Fig. 7a). They are added to aid with wave-soldering to PC boards and contribute no more than 0.1 pF to the overall value of a 100C or 100E series capacitor. These bands have razor sharp edges ($<$30 μm) that generate high electric fields resulting in corona discharge at the edges of the bands. To correct the problem, the bands were removed from the dielectric substrate with sandpaper, leaving only termination plates without sharp edges (Fig. 7b). A corona-suppressing coating (GC Electronics, p/n 10-4702 or 10-5002, other agents described in [44]) was then applied around the edges of the conductive plates to deny access to air molecules (Fig. 7c). The combination of these two steps improved the ^{15}N RF field to at least $f_1 = 71$ kHz in milliseconds-long pulses, with C_8 made of 100C series chips. Higher f_1 values were not attempted. To avoid damage to the probe, it is necessary to provide sufficient ventilation to elements of RF circuit both underneath and inside the variable temperature chamber, even if the sample is studied at room temperature. Neglecting to provide adequate ventilation (15–20 L/min) may lead to failure of fixed capacitors C_8 or C_0 from the internal heat build-up.

The orthogonal coil design can be expected to provide good intrinsic isolation between the ^{1}H and ^{15}N circuits. For the 600 MHz circuit shown in Fig. 5, transmission between the ^{15}N and ^{1}H ports at the ^{15}N frequency was measured to be less than -40 dB. The addition of $L_2 - C_4$, a small, half-turn low-voltage ^{1}H trap, at the entrance of the ^{15}N channel reduced transmission at the ^{1}H resonance frequency from -10 dB down to -35 dB. Due to its location in the circuit, the ^{1}H trap contributes almost no loss, extending the length of a 90° pulse by a mere 5%.

2.8. RF circuit for 900 MHz low-E probe

A ^{15}N–^{1}H flat-coil probe for the new 900 MHz ultra-wide bore magnet [45] was constructed using the same ^{1}H resonator and observe coil designs as those used in the 600 MHz low-E probe (Figs. 1C and 3A), with capacitance C_0 chosen to give $f_0 \sim 970$ MHz for the low-E resonator. However, the driving voltage required to produce the same RF field inside identical coils is proportional to spectrometer field strength (see Eq. (6)). Therefore the voltages in the 900 MHz probe are 1.5 times higher than at 600 MHz for the same experimental conditions, and so it was necessary to modify the RF circuit (shown in Fig. 8). Two fixed value chip capacitors C_9 were placed in series with the ^{15}N variable capacitors C_5, C_6, and C_7 to reduce voltage across these components. Without voltage dividers C_9 the air at the edge of the anode of C_6 or C_7 was ionized at a ^{15}N RF field approaching 55 kHz. With C_9 in place, we were able to achieve at least 70 kHz for 2 ms pulses. Other changes included moving ^{1}H matching trimmer capacitor C_1 (NMQM6G, 0.5–6 pF, Voltronics Corp.) in-line with the 50 Ω input and adding chip capacitor C_{3B} in parallel with C_3 to maintain electrical balance of the ^{1}H resonator. Because of increased voltage in the ^{1}H circuit, proper adjustment of the voltage balance at the ends of coil L_0 is crucial to the probe's ability to generate a high decoupling field.
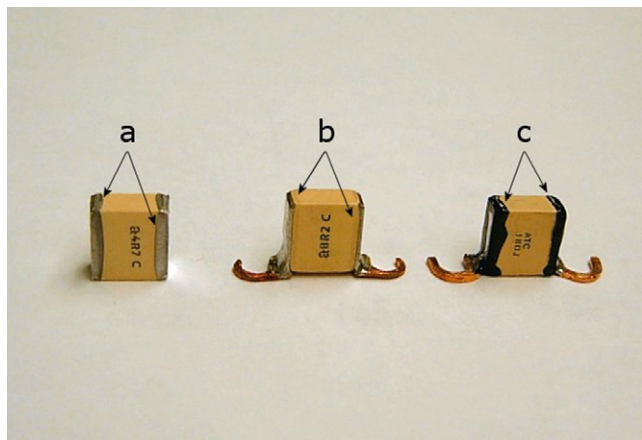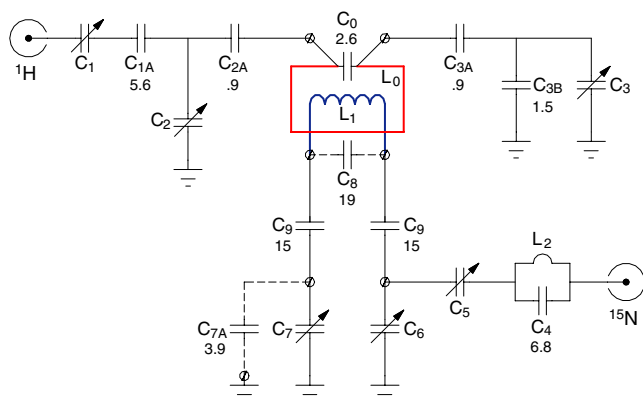

Fig. 7. Preparation of the ATC 100C series chip capacitor for service in the high-voltage location (C_{8A}). Razor sharp PC board bands (a) are filed off (b) and the remaining edges are covered with Corona Dope coating (c).

Fig. 8. RF circuit of the 900 MHz low-E ^{15}N–^{1}H flat-coil probe. Additional voltage dividers C_9 are inserted to protect ^{15}N variable capacitors and ^{1}H matching capacitor C_1 is located in-line with a 50 Ω cable. Coil inductance values are $L_0 \approx 10$ nH and $L_1 \approx 125$ nH.

3. Results

3.1. Comparing low-E and single-solenoid probes

Internal sample heating by the ^{1}H channel was measured in several large volume ^{15}N–^{1}H, PISEMA capable static probes for aligned samples. These probes include newly developed probes for 600 and 900 MHz that use a low-E coil assembly. The new probes were compared with the previously reported 600 MHz ^{15}N–^{1}H PISEMA probe employing a double-tuned 4-turn rectangular solenoid [16] and with a very similar version built for a 400 MHz spectrometer. The results of the comparison are presented in Table 2. All probes discussed in Table 2 were made for similar sample size. Different gap sizes ($gap = 6.4$ and 9.9 mm, Fig. 2) were tested for the low-E resonators at 600 MHz. Electric field presence in each probe was gauged by the ^{1}H 360° pulse lengths obtained with lipid bilayer and with non-lossy reference samples. Incident RF power was measured with an Agilent E4416A peak RF power meter by inserting a Werlatone C1795 directional coupler at the base of each probe *after* obtaining pulse length values. The fraction of ^{1}H input power heating the sample (α_{heat}) and sample heat deposition per kHz^2 of B_1 field (q_{heat}) were then determined from Eqs. (1) and (2). To get meaningful results using Eq. (1), the probes were balanced at the ^{1}H frequency before each τ_{360} measurement as described in Section 2.2. To determine the role that might be played by self-resonance effects, the self-resonance frequency f_{SR} of the 4-turn solenoid was measured to be 1044 and 985 MHz when loaded with non-lossy and biological reference samples, respectively. The effect of changing the sample on the electrical length n_λ of the solenoid is therefore only 5% (see Section 2.2). For single-coil probes at 400 and 600 MHz, it is safe to conclude that the changing from non-lossy to biological reference sample does not significantly affect the loss in the Cross–Waugh matching network. Sample dependent effects in the single-turn LGR will be even smaller than in the 4-turn solenoid. The mea-

surement of sample loss factor α_{heat} by means of Eq. (1) can therefore be considered accurate for probes discussed here. Table 2 also compares ^{1}H resonance shifts $\Delta f/f$ observed upon insertion of a hydrated bilayer sample as another useful indicator of electric field inside the coil. B_1 homogeneity $A_{810°}/A_{90°}$ in Table 2 was measured for both channels over the $6 \times 4 \times 9$ mm volume, using 100% neutral paraffinic oil and ^{15}N-labeled glycine. Table 2 includes the maximum sustainable ^{1}H decoupling field and comparison of RF fields produced by the ^{15}N channel at 700 W of input power.

The reduction in sample heating is best illustrated by comparing heat deposition coefficients q_{heat} in the 600 MHz low-E probe (lines 3 and 4 in Table 2) to those of the double-tuned 4-turn solenoid at the same frequency (line 2). Coefficient q_{heat}, a measure of RF power deposition in the biological sample at identical ^{1}H RF fields f_1, has been reduced by 17 times in low-E coil I and by 11 times in low-E coil II. Coil I, with its smaller value of the *gap* parameter, is more efficient and produces the least sample heating. However, coil II reaches a higher B_1. The much smaller shift of the ^{1}H resonance upon sample insertion $\Delta f/f$ also indicates reduced interaction with electric field in the new probes. Among other interesting parameters, the ^{15}N channel in the low-E probe is 73% more power efficient. We attribute this partly due to the elimination of lossy traps made possible by the orthogonal arrangement of RF coils, and partly because the number of turns in the observe solenoid is not restricted by ^{1}H wavelength, allowing for higher turn density. One might expect the ^{1}H power efficiency η of the low-E probe to be much worse than that of the solenoid due to the 3.3 times larger volume of the low-E resonator. However, the superior efficiency of the single resonance ^{1}H circuit in the low-E probe makes up for the difference in filling factor. As shown in Table 2, the low-E probe with coil I has the same ^{1}H efficiency as the double-tuned solenoid. The low-E probe with coil II is somewhat less efficient, which can be attributed to using more chip capacitors in the gap of a resonator. With three chips in series for each capacitor bridge that forms C_0, the total ESR of C_0 capacitors in coil II must be nearly 50% larger than in coil I with its two chips per bridge. Because of its larger size and shorter electrical length, the low-E ^{1}H resonator maintains excellent B_1 homogeneity over the sample region (Fig. 9A). The observe coil homogeneity (Fig. 9B) is similar or slightly lower than in the single-solenoid probe.

3.2. Sample heating at 900 MHz

For a given RF field f_1, the amount of ^{1}H power dissipated in the bilayer sample in a 900 MHz low-E probe is 4 times larger than in its 600 MHz counterpart (Table 2, coils II), yet it is still just 37% of the power dissipated in the double-tuned 4-turn solenoid probe at 600 MHz. A similar solenoid probe tuned to 900 MHz would provide
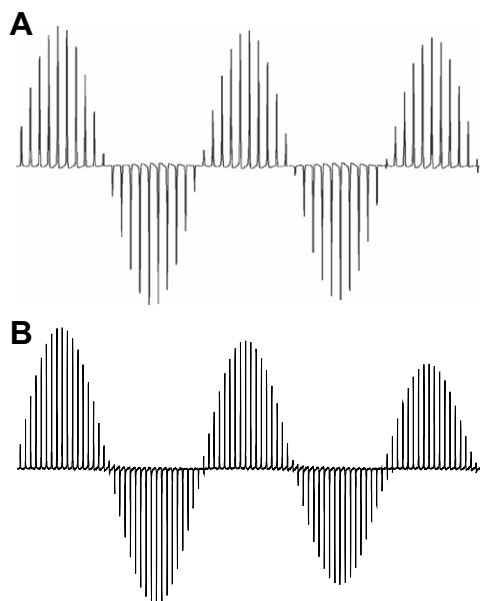
Fig. 9. B_1 nutation profile at ^{1}H (A) and ^{15}N (B) frequency across the $6 \times 4 \times 9$ mm rectangular volume in a 600 MHz low-E probe.

a better comparison with the 900 MHz low-E probe. While we were not successful in tuning this large volume solenoid to 900 MHz (its electrical length in air would become $>0.4\lambda$), the sample heating and RF homogeneity in such probe is expected to be significantly worse than at 600 MHz. It is worth noting that when the frequency is raised from 400 to 600 MHz, the RF heating in the lipid bilayers increases proportionally to f^2, as seen from measurements of q_{heat} in identical solenoids. But from 600 to 900 MHz, the increase in sample heating is larger than f^3, according to measurements with the same low-E coil. Despite this worrisome observation, the amount of ^{1}H sample heating in 900 MHz low-E probe is still slightly less than in the 400 MHz probe with a double-tuned 4-turn solenoid. To reduce any risk of dehydrating the sample, the 900 MHz decoupling field was not pushed above the minimum value sufficient for each sample under study. To date, the aligned samples studied in the 900 MHz

low-E probe have exhibited no signs of damage after demanding PISEMA experiments and we have been able to re-use them later for other experiments. Yet because of the large rise of heating in lipid membranes at 900 MHz, it is important to invest in further refinements to the low-E coil for use at ultra-high NMR fields.

3.3. RF fields in low-E probes at different frequencies

Table 3 lists power efficiencies of several low-E X–^{1}H flat-coil probes built for different spectrometer frequencies. All probes listed there have identical sample dimensions, with the exception of the small 600 MHz flat coil for sample-limited preparations (coil III). The third and fourth columns in Table 3 indicate the arrangement of C_0 chips (see Section 2.7) and the frequency f_0 to which the ^{1}H resonator was tuned before being installed into the probe, respectively. ^{1}H RF fields were measured using the 100% neutral paraffinic oil sample described above. Testing each probe with 10 ms pulses at the ^{1}H frequency ensured that arcing does not occur during the longest decoupling pulses used in our PISEMA experiments. A similar arcing test was done for the observe nuclei of interest (X = ^{15}N, ^{13}C, or ^{31}P) with pulse durations τ chosen from typical experiments. Pulses were repeated every 2 s (1 s for ^{31}P) with cooling air flow for the RF circuit set at 15–20 L/min. In spite of its large volume, the low-E resonator can deliver ^{1}H RF fields of up to 100 kHz at $f = 600$ MHz or less. Because voltage across the coil is proportional to B_0 (Eq. (6)), the ^{1}H field of the 900 MHz probe is limited by the possibility of arcing across the chip capacitors C_0 placed in the gap of the ^{1}H resonator. Near its 60 kHz f_1 limit, the 900 MHz ^{1}H coil must be well balanced to avoid ionization forming at either side of C_0. In the ^{15}N circuit of 600 and 900 MHz probes, corona discharge originally formed across the plates of C_8 capacitors at f_1 values close to 50 and 35 kHz, respectively. Modifying these chip capacitors as described in Section 2.7 of this article suppressed arcing and extended the limits of RF field achievable by the ^{15}N coil to at least 70 kHz.

Table 3
RF fields $f_1 = \omega_1/2\pi$ achieved in the X–^{1}H low-E flat-coil probes at various frequencies with different resonators

Field f MHz	Sample aperture mm	^{1}H coil *gap* mm	^{1}H coil f_0 MHz	X coil # of turns and L_1	^{1}H f_1 kHz at W $\tau = 10$ ms	^{31}P f_1 kHz at W $\tau = 1$ ms	^{13}C f_1 kHz at W $\tau = 2$ ms	^{15}N f_1 kHz at W $\tau = 2$ ms
300	$7.5 \times 5.5 \times 11$	9.9[II]	309	6t, 150 nH	100 at 243	100 at 150	100 at 212	84 at 517
500	$7.5 \times 5.5 \times 11$	9.9[II]	515	5t, 125 nH	105 at 300	100 at 255	110 at 400	80 at 700
600	$7.5 \times 5.5 \times 11$	6.4[I]	630	5t, 125 nH	76[a] at 156	—	—	71 at 700
600	$7.5 \times 5.5 \times 11$	9.9[II]	627	5t, 125 nH	100[a] at 342	80 at 150	—	71 at 700
600	$7 \times 3 \times 9$	3.0[III]	623	6t, 135 nH	100 at 170	—	—	90[a] at 495
900	$7.5 \times 5.5 \times 11$	9.9[II]	970	5t, 125 nH	60[a] at 176	—	—	70 at 800

[I,II]Large size low-E coils I and II elsewhere in the text, differing by the number of fixed capacitors.
[III]Small size low-E coil III for sample-limited preparations.
[1]^{1}H RF field was measured in 100% neutral paraffinic oil. No arcing occurred during pulses with duration τ chosen from typical experiments. Pulses were repeated every 1 s for phosphorous and every 2 s for other nuclei.
[a] Arcing occurs at higher RF field values.

3.4. PISEMA capabilities

The experimental capabilities of the $^{15}N-^{1}H$ low-E probes are demonstrated in Figs. 10 and 11. Experiments were conducted using a Bruker 600 MHz (14.1 T) wide bore spectrometer and the 900 MHz (21.2 T) ultra-wide bore NMR magnet at the National High Magnetic Field Laboratory equipped with a Bruker 900 MHz Avance Console. Low-E cross-coil assemblies with ^{1}H coil II were used at both fields. Fig. 10 shows 2D PISEMA spectra of ^{15}N-Leu sarcolipin (panel A) and ^{15}N-Leu phospholamban (panel B) in oriented DOPC/DOPE lipid bilayers obtained using the 600 MHz low-E probe. All 6 leucines present in SLN and 10 leucines in PLN are well resolved, with linewidths of ≈ 4 ppm and 1000 Hz in the ^{15}N chemical shift and $^{15}N-^{1}H$ dipolar coupling dimensions, respectively. Each spectrum was obtained in approximately 40 hours with cross-polarization and Lee–Goldberg RF fields of 68 kHz. In both spectra the observed PISA wheels are characteristic of α-helices having 3.6 residues per turn. Full analysis of PISEMA spectra on uniformly and selectively labeled SLN and PLN samples allowed for the topological characterization of both proteins within the lipid bilayer, providing an important first step toward the understanding of Ca^{2+}ATPase inhibition within cardiac myocytes [33,46]. Fig. 11 shows the 2D ^{15}N PISEMA spectrum of a single site ^{15}N-labeled amidated Piscidin-3 (^{15}N-Leu$_{20}$ P$_3$-NH$_2$, FIHHIFRGIVHAGRSIGRF[^{15}N-L$_{20}$]-TG- NH$_2$) oriented in DMPC/DMPG, obtained with the 900 MHz low-E probe [36]. As indicated by the ^{15}N chemical shift of 49.2 ppm, the amphipathic helix is aligned approximately parallel to the bilayer surface and is exposed to a very different dynamic environment than the SLN and PLN trans-

membrane helices described above. An inset allows for comparison of an expanded region of interest in the 900 MHz spectrum with a similar spectrum (blue overlay) obtained at 600 MHz. Both piscidin-3 spectra were collected with ^{1}H decoupling fields of 60 kHz at 40 °C. It took half the spectrometer time to collect the spectrum at 900 MHz. Notably, the ^{15}N NMR line in the chemical shift dimension of P$_3$-NH$_2$ is narrower at 900 than at 600 MHz, illustrating the advantage of higher field. Overall, this 900 MHz PISEMA spectrum shown here with 2.2 ppm chemical shift and 500 Hz $^{15}N-^{1}H$ dipolar linewidths is an excellent example of solid-state NMR study of a biological sample under physiologically relevant conditions. Similar quality 1D ^{15}N and 2D ^{15}N PISEMA spectra were previously reported for other single site ^{15}N-labeled piscidins with the 500 and 600 MHz low-E probes [37,36]. Studies in Figs. 10 and 11 illustrate the excellent spectral quality obtained with low-E probes when used with well-aligned sample preparations.

4. Conclusion and discussion

A special low-E solid-state NMR probe was developed for PISEMA studies of dielectrically lossy membrane protein preparations in order to minimize sample heating from ^{1}H irradiation. RF loss in the sample is minimized by employing a loop-gap resonator that produces a ^{1}H B_1 field with low conservative electric field and excellent homogeneity. A multi-turn solenoid closely matching the size and shape of the sample cell forms a sensitive ^{15}N observe coil inside the loop-gap resonator. Orthogonal coil placement simplifies the RF circuit by providing isolation between high and low-frequency channels and thus
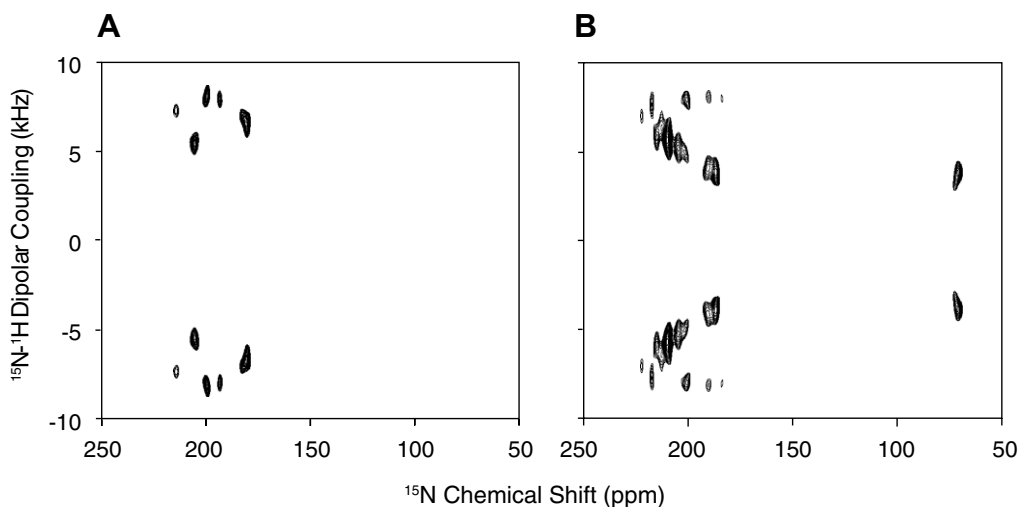

Fig. 10. 600 MHz 2D PISEMA spectra of ~3 mg of a ^{15}N-Leu-labeled SLN (A) and ~4 mg of ^{15}N-Leu-labeled PLN (B) in oriented DOPC/DOPE bilayers. Both PISEMA spectra were acquired at 5 °C with 12 t_1 increments, ~3 K scans and a recycle delay of 4 s. ^{1}H f_1 (decoupling) = 50 kHz, cross-polarization f_1 = 68 kHz, Lee–Goldberg f_1 = 68 kHz. The dipolar axis was not adjusted to account for the scaling factor of 0.81 arising from the application of phase-alternated Lee–Goldberg homonuclear decoupling [47,48]. ^{15}N chemical shifts were referenced to NH$_4$Cl at +41.5 ppm relative to liquid NH$_3$. Spectra are reprinted with permission from [33] (A) and [46] (B) (Copyright (2006) American Chemical Society).
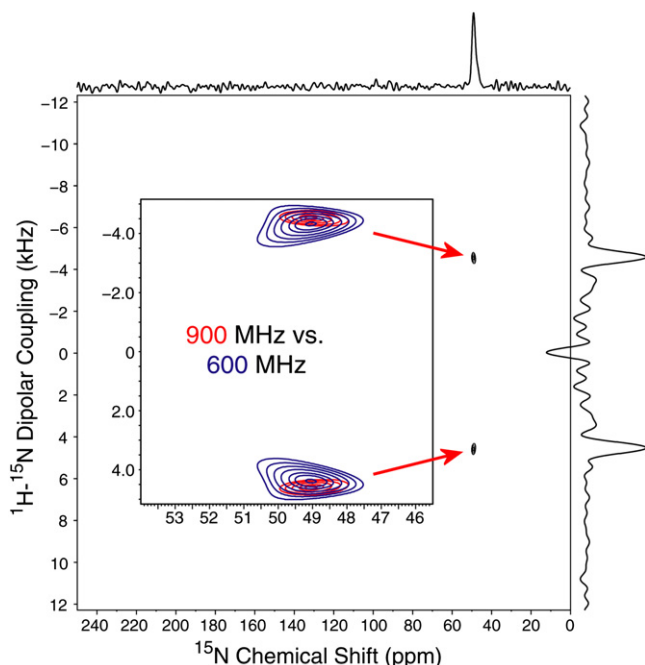
Fig. 11. Comparison of 900 and 600 MHz PISEMA spectra of piscidin-3 peptide. The slices are from the 900 MHz spectrum. 10 mg of single site ^{15}N-labeled amidated P$_3$-NH$_2$ were used (^{15}N-Leu$_{20}$ piscidin-3 in oriented DMPC/DMPG (3:1), 1:20 peptide to lipid ratio, pH 6). 900 MHz spectrum (red): 48 t_1 increments with 192 transients each, f_1 (decoupling) ~60 kHz, CP $f_1 \sim 45$ kHz. 600 MHz spectrum (blue): 48 t_1 increments with 256 transients each, f_1 (decoupling) ~60 kHz, CP $f_1 \sim 45$ kHz. Spectra were acquired at 40 °C with a recycle delay of 4 s. The dipolar axis in each spectrum was adjusted to account for the scaling factor of 0.81 arising from the application of phase-alternated Lee–Goldburg homonuclear decoupling [47,48]. ^{15}N chemical shifts were referenced to a saturated solution of ^{15}NH$_4$NO$_3$, at +22.3 ppm relative to liquid NH$_3$. Reprinted with permission from [36] (Copyright (2006) American Chemical Society).

avoiding multiple isolation traps—a source of major RF loss in single-coil circuits. The use of separate resonators allows the ^{1}H coil to be designed to reduce electric fields and improve ^{1}H homogeneity, whereas the observe solenoid, not limited by ^{1}H wavelength effects, can have more turns to gain sensitivity crucial for detection in dilute protein samples. Particularly significant for dilute preparations is the ability to accommodate larger sample volumes at higher frequency due to the short electrical length and high RF homogeneity of the loop-gap resonator.

The new, ^{15}N–^{1}H static flat-coil low-E probe for oriented proteins was compared to our previously reported flat-coil probe with a single, double-tuned solenoid of similar size [16]. Sample heating in lipid bilayers at the identical ^{1}H frequency and RF field levels ($\omega_1/2\pi$) was found to be reduced by more than a factor of 10 in the low-E probe. Despite the much smaller filling factor of the loop-gap resonator, its ^{1}H B_1 power efficiency (kHz^2/W) was measured to be comparable to the solenoid in the absence of sample loss and far better than in the solenoid for a lossy biological sample. For the ^{15}N channel, B_1 power efficiency was

measured to be 73% higher in the low-E probe than in the double-tuned solenoid.

Applications of low-E resonators to the study of membrane proteins in their native hydrated bilayer environment have been demonstrated at fields as high as 900 MHz. Lowering of electric fields in the sample coil has allowed for higher ^{1}H decoupling fields without dehydration or other damage to the sample, which is especially valuable at 900 MHz. The overall experimental time has been reduced due to a shorter thermal recovery period (when sample T_1 permits) and less time spent adjusting CP parameters for each sample. These new probes are now routinely used for ^{15}N PISEMA studies of dilute membrane proteins at 900 and 600 MHz spectrometers in the National High Magnetic Field Laboratory. Scientists who would like to use these probes are invited to apply to the NHMFL.

The low-E probes described here are expected to benefit solid-state NMR of other biological and hydrated objects, especially at ultra-high fields such as 900 MHz. Applications may include highly hydrated solid samples such as nanocrystals in a mother solution, collagens, elastins, bicelles, hydrated polymers, etc. The low-frequency solenoid need not be limited to the rectangular and stationary design demonstrated here. A scaled-down version of this design made with a round solenoid can be used for MAS applications or to study proteins in bicelle preparations. ^{19}F–^{1}H NMR of biological solids, where both ^{19}F and ^{1}H pulses contribute to sample heating, is another area we expect to benefit from the orthogonal low-E design. Since the Larmor frequencies of ^{19}F and ^{1}H are only 6% apart, achieving good isolation between channels is not trivial in ^{19}F–^{1}H single-coil circuits. On the other hand, a ^{19}F–^{1}H circuit that utilizes nested and orthogonal loop-gap resonators will reduce electric fields at both frequencies and simplify isolation between the ports. This design is not covered in this manuscript and will be discussed elsewhere.

Acknowledgments

parts used in the probes, Brenna S. Vollmar for help with sample preparation, Dr. Raiker Witter and Kiran K. Shetty for help with probe testing, Dr. Riqiang Fu for help with PISEMA setup, Dr. Yit A. Lim, Dr. Werner Maas, and Dr. F. David Doty for helpful discussions.

Appendix A. Using solid angles to express axial component of solenoid magnetic field

The axial component of magnetic field produced by a solenoid of *arbitrary* cross-section at *any* point A in space can be conveniently expressed in terms of the total solid angle Ω at which the current flow is seen by an observer at point A. Consider any small area element dS on the surface of a solenoid aligned with the x-axis (Fig. 12). From the Bio-Savart law, the total magnetic field vector $d\vec{B}$ produced by this element at the observation point A is given by

$$d\vec{B} = \mu_0 \frac{\vec{i} \times \vec{r}}{4\pi r^3} \, dS,$$

where $\vec{r}$ is a vector from element dS to the observation point A and $\vec{i}$ is the current density. The axial component of magnetic field is obtained by projecting $d\vec{B}$ onto the unit vector $\hat{x}$ collinear with the solenoid axis:

$$d\vec{B}_x = \hat{x} \cdot d\vec{B} = \mu_0 \frac{\hat{x} \cdot [\vec{i} \times \vec{r}]}{4\pi r^3} \, dS = \mu_0 \frac{[\hat{x} \times \vec{i}] \cdot \vec{r}}{4\pi r^3} \, dS$$

Because $\hat{x} \times \vec{i} = -\hat{n}i$,

$$d\vec{B}_x = -\mu_0 i \frac{(\hat{n} \cdot \vec{r})}{4\pi r^3} \, dS = \mu_0 i \frac{d\Omega}{4\pi},$$

where $d\Omega = -\frac{(\hat{n} \, dS \cdot \vec{r})}{r^3}$ is the solid angle at which the area element dS is seen from observation point A. If the surface current density value and direction are constant, then the total axial component of magnetic field at point A is simply
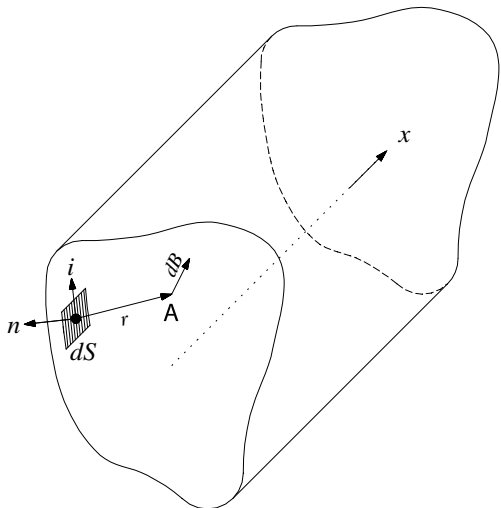

Fig. 12. Illustration to Appendix A: derivation of axial magnetic field $B_x(\vec{r})$ for a solenoid of arbitrary cross-section using solid angles.

$$\vec{B}_x = -\frac{\mu_0 i}{4\pi} \int d\Omega = \mu_0 i \frac{\Omega}{4\pi}. \tag{10}$$

Eq. (10) is valid for all points both inside and outside of the solenoid. For a very long solenoid, the field inside is simply $\vec{B}_x = \mu_0 i$. At the end of a long solenoid $\Omega = 2\pi$, hence $\vec{B}_x = \frac{1}{2}\mu_0 i$.

For a finite solenoid of round cross-section with diameter $2a$ and length $2b$, from any point A on the axis, the winding subtends a solid angle $\Omega = 2\pi(\cos\varphi_1 - \cos\varphi_2)$, where ϕ_1 and ϕ_2 are the regular angles at which the end rings are seen with respect to x-axis:

$$B_x(x,0,0) = \frac{1}{2}\mu_0 i \left(\frac{b+x}{\sqrt{(b+x)^2 + a^2}} - \frac{b-x}{\sqrt{(b-x)^2 + a^2}} \right).$$

The field at the center of the finite round solenoid ($x = 0$) is therefore $B_x(0,0,0) = \mu_0 i \dfrac{b}{\sqrt{b^2 + a^2}}$. From the center of a circular loop of wire of diameter d and current I having radius $a \gg d$, the solid angle subtended by the wire is $\Omega \approx 2\pi d/a$, and the field in the center becomes a familiar formula $B_x(0,0,0) = \dfrac{\mu_0 I}{2a}$.

Now, consider a finite solenoid of rectangular cross-section with sides $2a$ and $2b$ and length $2c$. From a point on the axis $(x,0,0)$, the solenoid subtends the solid angle $\Omega = 4\pi - \Omega_1 - \Omega_2$, where Ω_1 and Ω_2 are the solid angles of the rectangular openings at $x = \pm c$.

$$\Omega_1 = \int_{-a}^{a} \int_{-b}^{b} dy, dz \, \frac{(\hat{n} \cdot \hat{x})}{r^2} = \int_{-a}^{a} \int_{-b}^{b} \frac{dy\,dz(c+x)}{\left((c+x)^2 + y^2 + z^2\right)^{3/2}}$$

$$= 4\tan^{-1}\left(\frac{ab}{(c+x)\sqrt{a^2 + b^2 + (c+x)^2}} \right),$$

$$\Omega_2 = 4\tan^{-1}\left(\frac{ab}{(c-x)\sqrt{a^2 + b^2 + (c-x)^2}} \right).$$

The field at the center of such a rectangular solenoid is

$$B_x(0,0,0) = \mu_0 i \left(1 - \frac{2}{\pi}\tan^{-1}\frac{ab}{c\sqrt{a^2 + b^2 + c^2}} \right). \tag{11}$$

References

[1] R.W. Martin, E.K. Paulson, K.W. Zilm, Design of a triple resonance magic angle sample spinning probe for high field solid state nuclear magnetic resonance, Rev. Sci. Instrum. 74 (2003) 3045–3061.

[2] S.V. Dvinskikh, V. Castro, D. Sandström, Heating caused by radiofrequency irradiation and sample rotation in ^{13}C magic angle spinning NMR studies of lipid membranes, Magn. Reson. Chem. 42 (2004) 875–881.

[3] C. Li, Y. Mo, J. Hu, E.Y. Chekmenev, C. Tian, F.P. Gao, R. Fu, P.L. Gor'kov, W.W. Brey, T.A. Cross, Analysis of RF heating and sample

stability in aligned static solid state NMR spectroscopy, J. Magn. Reson. 180 (2006) 51–57.

[4] J.J. Led, S.B. Petersen, Heating effects in ^{13}C NMR spectroscopy on aqueous-solutions caused by proton noise decoupling at high-frequencies, J. Magn. Reson. 32 (1978) 1–17.

[5] D.I. Hoult, P.C. Lauterbur, Sensitivity of the zeugmatographic experiment involving human samples, J. Magn. Reson. 34 (1979) 425.

[6] D.G. Gadian, F.N.H. Robinson, Radiofrequency losses in NMR experiments on electrically conducting samples, J. Magn. Reson. 34 (1979) 449–455.

[7] F.D. Doty, G. Entzminger, Y.A. Yang, Magnetism in high resolution NMR probe design. II: HR MAS, Concepts Magn. Reson. 10 (4) (1998) 239–260.

[8] J.B.D. de Lacaillerie, B. Jarry, O. Pascui, D. Reichert, "Cooking the sample": radiofrequency induced heating during solid-state NMR experiments, Solid State Nucl. Magn. Reson. 28 (2005) 225–232.

[9] F.D. Doty, J. Kulkarni, C. Turner, G. Entzminger, A. Bielecki, Using a cross-coil to reduce RF heating by an order of magnitude in triple-resonance multinuclear MAS at high fields, J. Magn. Reson. 182 (2) (2006) 239–253.

[10] A.C. Wang, A. Bax, Minimizing the effects of radiofrequency heating in multidimensional NMR experiments, J. Biomol. NMR 3 (6) (1993) 715–720.

[11] H. Kugel, Improving the signal-to-noise ratio of NMR signals by reduction of inductive losses, J. Magn. Reson. 91 (1) (1991) 179–185.

[12] B. Bechinger, S.J. Opella, Flat-coil probe for NMR spectroscopy of oriented membrane samples, J. Magn. Reson. 95 (1991) 585–588.

[13] N.C. Nielsen, P. Daugaard, V. Langer, J.K. Thomsen, S. Nielsen, O.W. Sorensen, H.J. Jakobsen, A flat-coil NMR probe with hydration control of oriented phospholipid bilayer samples, J. Biomol. NMR 5 (1995) 311–314.

[14] C. Tian, P.F. Gao, L.H. Pinto, R.A. Lamb, T.A. Cross, Initial structural and dynamic characterization of the M2 protein trans-membrane and amphipatic helices in lipid bilayers, Protein Sci. 12 (2003) 2597–2605.

[15] J.K. Rainey, J.S. DeVries, B.D. Sykes, A rotatable flat coil for static solid-state nuclear magnetic resonance spectroscopy, Rev. Sci. Instrum. 76 (2005).

[16] P.L. Gor'kov, E.Y. Chekmenev, R. Fu, J. Hu, T.A. Cross, M. Cotten, W.W. Brey, A large volume flat coil probe for oriented membrane proteins, J. Magn. Reson. 181 (2006) 9–20.

[17] R.W. Dykstra, A technique to increase NMR sensitivity for conductive solutions, J. Magn. Reson. 84 (2) (1989) 388–391.

[18] A.E. Kelly, H.D. Ou, R.S. Withers, V. Dötsch, Low-conductivity buffers for high-sensitivity NMR measurements, J. Am. Chem. Soc. 124 (40) (2002) 12013–12019.

[19] R. McNamara, C.H. Wu, S.J. Opella, Instrumental techniques for low-temperature solid-state NMR studies of peptides and proteins, J. Magn. Reson. 100 (1992) 559–566.

[20] D.W. Alderman, D.M. Grant, Efficient decoupler coil design which reduces heating in conductive samples in superconducting spectrometers, J. Magn. Reson. 36 (1979) 447–451.

[21] W.N. Hardy, L.A. Whitehead, Split-ring resonator for use in magnetic-resonance from 200 to 2000 MHz, Rev. Sci. Instrum. 52 (1981) 213–216.

[22] W. Froncisz, J.S. Hyde, The loop-gap resonator—a new microwave lumped circuit electron-spin-resonance sample structure, J. Magn. Reson. 47 (1982) 515.

[23] T.M. Grist, J.S. Hyde, Resonators for in-vivo P-31 NMR at 1.5T, J. Magn. Reson. 61 (1985) 571.

[24] L.D. Hall, T. Marcus, C. Neale, P. Powell, J. Sallos, S.L. Talagala, A modified split-ring resonator probe for NMR imaging at high-field strength, J. Magn. Reson. 62 (1985) 525.

[25] J.P. Hornak, T.L. Ceckler, R.G. Bryant, P-31 NMR spectroscopy using a loop gap resonator, J. Magn. Reson. 68 (1986) 319.

[26] F.H. Larsen, P. Daugaard, H.J. Jakobsen, N.C. Nielsen, Improving RF field homogeneity in solid-state MAS NMR using a loop-gap resonator, J. Magn. Reson. A 115 (1995) 283–286.

[27] D.G. Cory, J.T. Lewandowski, W. Maas, NMR probe for cross-polarization experiments, United States Patent #5,539,315, July 23, 1996.

[28] S.C. Grant, L.A. Murphy, R.L. Magin, G. Friedman, Analysis of multilayer radio frequency microcoils for nuclear magnetic resonance spectroscopy, IEEE Trans. Magn. 37 (2001) 2989–2998.

[29] J.A. Stringer, C.E. Bronnimann, C.G. Mullen, D.H. Zhou, S.A. Stellfox, Y. Li, E.H. Williams, C.M. Rienstra, Reduction of RF-induced sample heating with a scroll coil resonator structure for solid-state NMR probes, J. Magn. Reson. 173 (1) (2005) 40–48.

[30] C. Mullen, J. Stringer, K. Mehr, Multiple tuned scroll coil, United States Patent #7,081,753, July 25, 2006.

[31] E.K. Paulson, R.W. Martin, K.W. Zilm, Cross polarization, radio frequency field homogeneity, and circuit balancing in high field solid-state NMR probes, J. Magn. Reson. 171 (2004) 314–323.

[32] A. Odermatt, P.E.M. Taschner, S.W. Scherer, B. Beatty, V.K. Khanna, D.R. Cornblath, V. Chaudhry, W.C. Yee, B. Schrank, G. Karpati, M.H. Breuning, N. Knoers, D.H. MacLennan, Character-ization of the gene encoding human sarcolipin (SLN), a proteolipid associated with SERCA1: absence of structural mutations in five patients with Brody disease, Genomics 45 (1997) 541–553.

[33] J.J. Buffy, N.J. Traaseth, A. Mascioni, P.L. Gor'kov, E.Y. Chekme-nev, W.W. Brey, G. Veglia, Two-dimensional solid-state NMR reveals two topologies of sarcolipin in oriented lipid bilayers, Biochemistry 45 (36) (2006) 10939–10946.

[34] U. Silphaduang, E.J. Noga, Antimicrobials—peptide antibiotics in mast cells of fish, Nature 414 (2001) 268–269.

[35] X. Lauth, H. Shike, J.C. Burns, M.E. Westerman, V.E. Ostland, J.M. Carlberg, J.C. Van Olst, V. Nizet, S.W. Taylor, C. Shimizu, P. Bulet, Discovery and characterization of two isoforms of moronecidin, a novel antimicrobial peptide from hybrid striped bass, J. Biol. Chem. 277 (2002) 5030–5039.

[36] E.Y. Chekmenev, S.M. Jones, Y.N. Nikolayeva, B.S. Vollmar, T.J. Wagner, P.L. Gor'kov, W.W. Brey, M.N. Manion, K.C. Daugherty, M. Cotten, High-field NMR studies of molecular recognition and structure–function relationships in antimicrobial piscidins at the water–lipid bilayer interface, J. Am. Chem. Soc. 128 (16) (2006) 5308–5309.

[37] E.Y. Chekmenev, S.M. Jones, Y.N. Nikolayeva, B.S. Vollmar, T.J. Wagner, M.N. Manion, K.C. Daugherty, B.P. Kyriss, D.R. Jacobsen, P.L. Gor'kov, W.W. Brey, A.J. Auman, M.A. Ellard-Ivey, M. Cotten, Investigating molecular recognition and biological function at interfaces using piscidins, antimicrobial peptides from fish, Biochim. Biophys. Acta 1758 (2006) 1359–1372.

[38] H.E. Alper, D. Bassolino, T.R. Stouch, Computer simulation of a phospholipids monolayer-water system: influence of long range forces on water structure and dynamics, J. Chem. Phys. 98 (1993) 9798–9807.

[39] D.M. Willard, R.E. Roter, N.E. Levinger, Dynamics of polar salvation in Lecithin/water/cyclohexane reverse micelles, J. Am. Chem. Soc. 120 (1998) 4151–4160.

[40] W. Lu, J. Kim, W. Qiu, D. Zhong, Femtosecond studies of tryptophan salvation: correlation function and water dynamics at lipid surfaces, Chem. Phys. Lett. 388 (2004) 120–126.

[41] V.R. Cross, R.K. Hester, J.S. Waugh, Single coil probe with transmission-line tuning for nuclear magnetic double-resonance, Rev. Sci. Instrum. 47 (1976) 1486–1488.

[42] Z. Zhang, P.C. Hammel, G.J. Moore, Application of a novel rf coil design to the magnetic resonance force microscope, Rev. Sci. Instrum. 67 (9) (1996) 3307–3309.

[43] O. Stuhlman Jr., S. Githens Jr., The magnetic field of a solenoid oscillating at radio frequencies, Rev. Sci. Instrum. 3 (1932) 561–571.

[44] F.D. Doty, G. Entzminger, Y.A. Yang, Magnetism in high resolution NMR probe design. I: general methods, Concepts Magn. Reson. 10 (3) (1998) 133–156.

[45] R. Fu, W.W. Brey, K. Shetty, P.L. Gor'kov, S. Saha, J.R. Long, S.C. Grant, E.Y. Chekmenev, J. Hu, Z. Gan, M. Sharma, F. Zhang, T.M. Logan, A. Edison, A. Blue, I. Dixon, Ultra-wide bore 900 MHz high-

resolution NMR at the national high magnetic field laboratory, J. Magn. Reson. 177 (2005) 1–8.

[46] N.J. Traaseth, J.J. Buffy, J. Zamoon, G. Veglia, Structural dynamics and topology of phospholamban in oriented lipid bilayers using multi-dimensional solid-state NMR, Biochemistry 45 (46) (2006) 13827–13834.

[47] C.H. Wu, A. Ramamoorthy, S.J. Opella, High-resolution heteronuclear dipolar solid-state NMR spectroscopy, J. Magn. Reson. A 109 (1994) 270–272.

[48] Z.T. Gu, S.J. Opella, Three-dimensional ^{13}C shift/^{1}H-^{15}N Coupling/^{15}N shift solid-state NMR correlation spectroscopy, J. Magn. Reson. 138 (1999) 193–198.